Parallel Imaging Techniques in Functional MRI

Xavier Golay, PhD, Jacco A. de Zwart, PhD,† Yi-Ching Lynn Ho, MS,* and Yih-Yian Sitoh, MD**

Abstract: Originally developed for increased scanning velocity in cardiac imaging, parallel imaging (PI) techniques have recently also been applied for the reduction of artifacts in single-shot techniques. In functional brain imaging (fMRI) techniques, PI has been used for several purposes. It has been applied to reduce the distortions caused by the length of the echo-planar imaging readout, diminution of the gradient-related acoustic noise, as a means to increase acquisition speed or to increase the achievable brain coverage per unit time. In this article, the different applications of PI techniques in fMRI are reviewed, together with the basic theoretical background and the recently developed hardware necessary to achieve rapid, high signal-to-noise ratio PI-fMRI.

Key Words: parallel imaging, SENSE, SMASH, fMRI, BOLD, arterial spin labeling, VASO

(*Top Magn Reson Imaging* 2004;15:255–265)

PARALLEL IMAGING IN BLOOD OXYGEN-LEVEL DEPENDENT (BOLD) FMRI

Dedicated Hardware

In the first papers that described the use of parallel imaging (PI) for neurologic applications, ad hoc arrays of receiver coils were used, manually assembled from surface coil elements placed around the head. Usually, the number of coils was limited (from three to six).[1,2] These setups were useful in getting preliminary PI images of the brain but were suboptimal in many ways.

Initially, these phased array coils were using rather large individual elements placed relatively far away from the tissue of interest. Results from simulations and experiments suggest that when sample noise is the dominant noise source, the image signal-to-noise ratio (SNR) increases with the number of coil elements[3,4] for arrays of surface coils fully covering an object of interest. This increase in SNR is mainly found in the peripheral brain, whereas SNR in deeper brain structures stays virtually constant. Therefore, PI seems to be a useful tool for brain imaging, as head geometry allows a very good coverage of the region of interest with a relatively large number of small surface coils that can be nicely arranged around the head.

Over the last few years, a number of different coil designs have appeared, all aimed at maximizing both SNR and the achievable PI acceleration factor R. De Zwart et al. demonstrated the use of a dedicated phased array coil with either eight[3] or sixteen[5] elements for 1.5 T and 3.0 T imaging, respectively. The coil elements were placed around the head in a single row. In this particular design, the anterior coil elements were designed shorter than the posterior elements to achieve whole brain coverage while maintaining the largest possible visual field for the subject. With the 8-element design, a 2.7-fold improvement in SNR was achieved compared with the standard quadrature birdcage transmit/receive coil and the average geometrical noise amplification factor (g factor, always ≥ 1.0, best if $= 1.0$[6]) was of 1.06 and 1.38 for SENSE[6] reduction factors $R = 2$ and $R = 3$, respectively, at 1.5 T. At 3.0 T, the increase in SNR was 1.87-fold for the 16-element array when compared with a simulated single-element coil with the same geometry, and ranged from 2- to 6-fold when compared with the standard birdcage. However, results from their simulations show that the increase in SENSE performance is limited for SENSE reduction factor $R = 2$ when going from 8 to 16 channels. On the other hand, the use of 16 channels versus 8 channels is significantly more beneficial for higher acceleration factors (such as $R = 3$ and above).

Moving to an even larger numbers of coils, Yang et al.[7] simulated and built a 12-receiver "dome-like" head coil optimized for PI at 3.0 T. By comparing the g maps at high acceleration factors using a 6- or 12-element phased array coil, they concluded that more coils are preferable to keep the average g factor low, in good agreement with de Zwart et al.[5]

The same group also studied the possibility of building an 8-channel hybrid transmit/receive phased array coil suitable for head imaging at 3.0 T and 4.0 T whole-body MRI systems.[8] In this design, while the transmit coil is electrically separated from the receive coils, they are physically integrated into a single package. The transmitter portion of the coil is comprised of a 16-leg birdcage resonator, while the receiver part of the coil consists of 8 nonoverlapping mutually decoupled elements in the shape of an open dome design. The average g values varied from 1.15 for $R = 2$ to 4.09 for $R = 4$ at 3.0 T, and

From the *Department of Neuroradiology, National Neuroscience Institute, Singapore; and the †Advanced MRI section, LFMI, NINDS, National Institutes of Health, Bethesda, MD.

Reprints: Xavier Golay, PhD, Department of Neuroradiology, National Neuroscience Institute, 11 Jalan Tan Tock Seng, Singapore, 308433 (e-mail: Xavier_Golay@nni.com.sg).

from 1.09 for $R = 2$ to 3.19 for $R = 4$ at 4.0 T. The authors explained the slight improvements at 4.0 T by the larger phase variations of the B_1 field at higher field strength.[7] In similar fashion, Wiggins et al.[9] used a detunable Transverse Electro-Magnetic (TEM) coil combined with a separate flexible 8-element array.

Adriany et al.[10] proposed another version of strip-line transceiver coils for ultra-high field (4.0 T and 7.0 T) PI-imaging using either four or eight elements. Using their coil, no resonance peak split was observed and the coils could be tuned and matched individually for each subject. Furthermore, by adjusting the transmit phase and amplitude of each coil element independently, they were able to achieve good PI performance while obtaining additional "radio frequency (RF) shimming capabilities," that is the possibility to increase the local B1 homogeneity of the applied RF pulses by counterbalancing the "dielectric effects," which are more important at these higher field strengths. At $R = 3$, they obtained an average geometry factor of 1.41 when phase encoding was reduced along the long axis and 1.65 when phase encoding was reduced along the short axis with a four-channel array. The eight-channel array achieved an average g factor of 1.28 for $R = 4$, corroborating the fact that the maximum obtainable reduction factor indeed increases with field strength. Recently, based on their previous work on send-receive array coil designs for 7.0 T, the same authors increased the number of independent coils to 32 and concluded that gains in SNR at high acceleration factor R can still be realized in human head imaging at 7 T, with $R = 5$ to 6 in one dimension or $R = 8$ to 12 in two dimensions with acceptable g factors.[11]

Other groups have proposed different solutions for PI at ultra-high field. For example, Zhang et al.[12] exploited microstrip transmission line technology to design an RF coil array characterized by an extremely broad frequency tuning range from 115 MHz to 310 MHz in loaded condition. This specific coil array could be used for proton MR applications at different field strengths ranging from 3.0 T to 7.0 T and/or to study both ^{1}H and ^{31}P nuclei at 7.0 T field strength. Using another new technology, Junge et al.[13] demonstrated the potential of using current-sheet-antenna-array coils for high field MRI. With this technology, increasing the number of array elements is expected to yield additional benefits regarding SNR and B_1 homogeneity.

Finally, a few groups recently studied the potential of using triangular shaped[14,15] and other specially shaped multi-coil elements[16] to increase the benefits of using multidimensional PI in the head with conventional axial acquisitions.[17]

The coils described above were developed for research purposes with no or limited commercial availability. However, all three major manufacturers of clinical imagers currently support the use of the same FDA-approved 8-element phased array coil[18] as the PI-optimized head coil.

Use of Parallel Imaging for Artifact Reduction in Fast Readouts

The first PI techniques published were developed in cardiac groups as a means to increase scanning velocity.[19,20] It soon appeared that such techniques could also be used to reduce artifacts due to k-space blurring[21,22] and off-resonance effects[23] incurred during long readout periods, such as during EPI acquisitions. These effects are particularly present in diffusion-weighted imaging, and for this reason, PI was first implemented for this particular imaging technique.[2,24] Furthermore, both effects scale with the main magnetic field B_0, making the transition to higher field strengths challenging.[25] As an example of such geometric distortions at 3.0 T, Figure 1 demonstrates the distortion reduction achieved in single T2*-weighted images when going from no acceleration factor ($R = 1$) to $R = 2$ and $R = 3$ on a mid-brain axial slice. Note the reduction of the "elongation" effect with increasing acceleration factors.

The principal benefit of PI on the single-shot EPI readout resides in the fact that by increasing the spacing of phase-encoding steps in k-space, and subsequently reducing the number of steps required to cover a given area of k-space, it boosts the speed of acquisition in the phase encoding direction. In this fashion, it reduces the artifacts due to transverse relaxation and spin diffusion through field gradients. Jaermann et al.[25] recently described theoretically the quantitative effects of PI on both the averaged phase encoding gradient strength $\overline{G_{PE}}$ and the SNR efficiency in such sequences.

In short, it was found that since the spatial resolution in the phase encoding direction is inherently limited by T2 (or T2*), the blurring kernel should be equal to a filter, whose width scales inversely with $\overline{G_{PE}}$. Therefore, PI should increase the intrinsically achievable resolution in EPI by a factor equal to the reduction factor R. As for susceptibility artifacts, the distribution of frequency offsets within the reconstructed image will result in a shift along the phase encoding direction, leading to distortions and blurring effects. This shift will scale with the ratio of the frequency offset over $\overline{G_{PE}}$. Hence, PI will accordingly reduce it by a factor R.

As for SNR efficiency, taking into account the potential increase in SNR due to a reduced echo time in such sequences, it was found that the SNR in diffusion-weighted EPI can be expressed by[25]:

$$SNR_{PI} = \frac{\exp\left(-\frac{t_{acq}\,(1/R-1)+2\cdot c\cdot(R-1)}{T2}\right)}{g\sqrt{R}}\cdot SNR_{full} \qquad (1)$$

with t_{acq} being the total length of the EPI readout, while R is the speeding (or reduction) factor, g is the geometry factor,[20] and c is a constant term depending on the effective diffusion weighting. The important message from this equation is

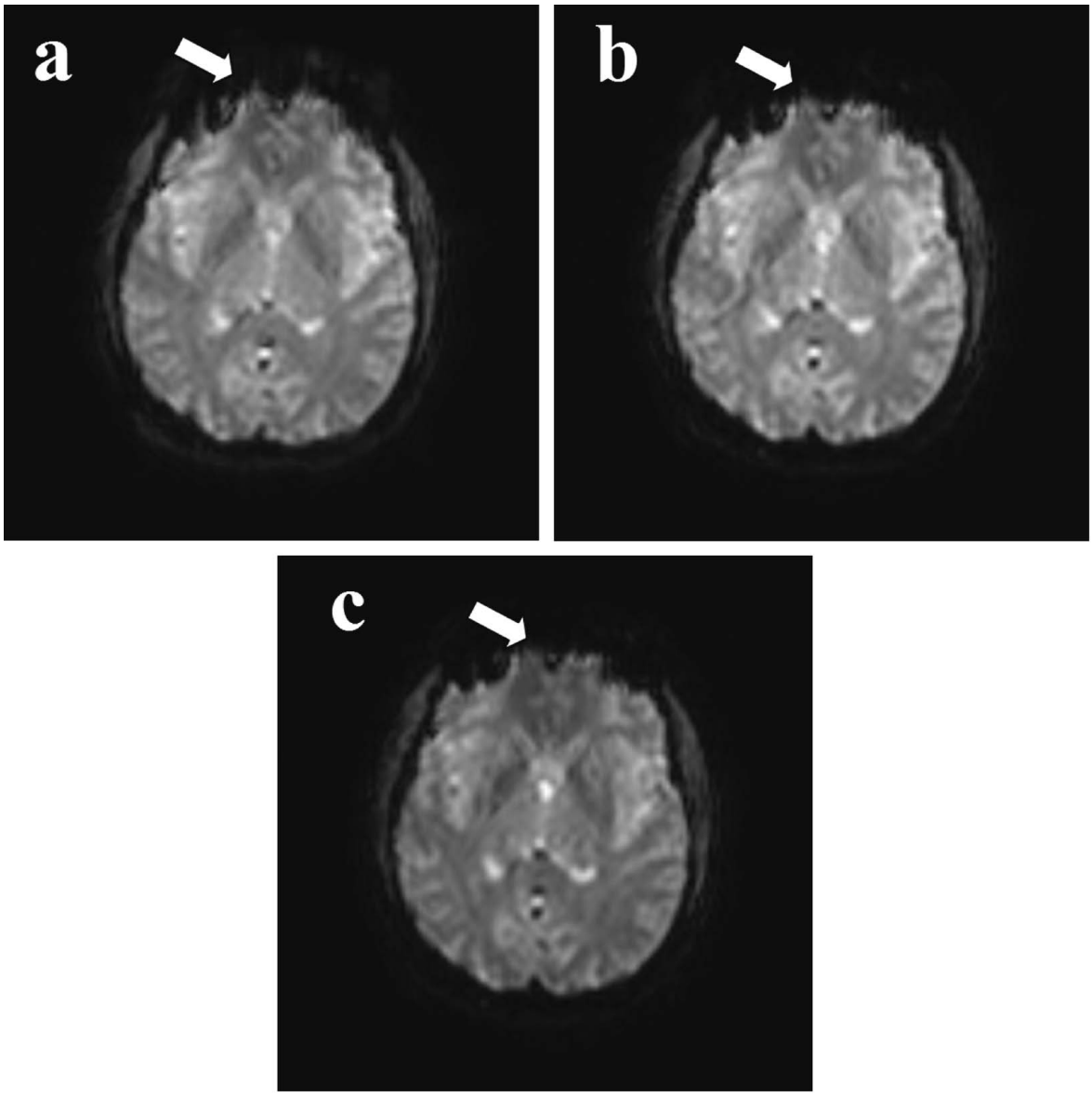

FIGURE 1. Single-shot EPI without SENSE (A), with $R = 2$ (B), and $R = 3$ (C) at 3.0 T. Other parameters were: TR = 2000 milliseconds, TE = 30 milliseconds, FA = 90°, matrix = 80 × 80, slice thickness = 4 mm. Please note the reduction of the elongation effect with increasing acceleration factor (*arrows*). Image a was reconstructed using a "SENSE factor 1" reconstruction to allow better signal comparison and more homogeneous tissue appearance.

that contrary to intuition, the SNR in PI does not have to be smaller than that of full *k*-space acquisition. Different effects will produce similar behavior in fMRI, during which multiple volumes are acquired over minutes, and for which the SNR per unit time becomes the most important factor in the statistical analysis (see *SNR Considerations and Statistical Analysis*).

Several works have investigated the use of PI in fMRI, with reductions in distortion as their primary goal.[26,27] First, Weiger et al.[26] implemented a Spiral-SENSE[28] technique and used it in simple (visual and motor), as well as more elaborate (taste) functional experiments. All the experiments were performed using block paradigms. In their experiments, the SNR and signal-to-fluctuation-noise ratio were generally diminished by 20% and 13%, respectively, when using a reduction factor $R = 2$, shortening in such cases the readout window from 36 milliseconds to 18 milliseconds for an in-plane resolution of 3 × 3 mm. However, in their study, this SENSE reduction factor did not affect the detection power of the activation, and the number of activated voxels remained more or less constant over the experiments. An important result of their study was

the demonstration of the ability of PI to recover part of the signal loss present in the deep orbitofrontal areas (involved in the taste experiments) due to the reduced sensitivity to magnetic field homogeneity. Similar results were gathered more recently using an odor-based stimulus with an optimized SENSE sequence and a z-shim preparation gradient on a 30° tilted acquisition.[29,30] Finally, the Weiger et al. successful combination of PI with spiral imaging opened up the route for the recently developed reversed SENSE-spiral technique, which was also used in a similar context.[31]

Preibisch et al.[27] on the other hand used a more straightforward SENSE-EPI approach and performed a thorough evaluation of the variation of the SENSE factor on the intrinsic SNR as well as the detection power using simple motor tasks. Their study was performed at 1.5 T on a standard clinical scanner. Their results can be summarized as follows: At intermediate acceleration factor $R = 2$, they were able to increase the number of slices per unit of time at high spatial resolution, as well as decrease the distortions without significant loss in statistical power. At higher R factors, they experienced a rapid loss in SNR. This result seems to be in line with the most recent studies on the maximum achievable acceleration factors as a function of field strength,[20,32] which state that for high R values, the imaging performances will deteriorate, due to exponential augmentation of the geometry factor g. The transition from optimal to deteriorating imaging performance will take place at an increased R for higher magnetic field strength B_0, and therefore allows a nearly linear increase in maximal R factor with respect to the main magnetic field.

In accordance with these theoretical studies, Schmidt et al.[33] and Morgan et al.[34] used SENSE-EPI at 3.0 T and found optimal acceleration factors between 2 and 3 at this magnetic field strength, while Little et al.[35] found no detrimental use in activation detection with a reduction factor of 3 using a k-space-based reconstruction method (GRAPPA[36]). Finally, it was recently demonstrated that the acquisition of T2*-weighted images with an acceleration factor $R = 4$ is possible at 7.0 T.[37]

Fast PI-fMRI Techniques for Spatial or Temporal Resolution Increases

Generally speaking, the increase in coverage obtainable by the use of PI in fMRI is limited in T2*-based fMRI methods, as relatively long echo times (TE) are used (typically TE ~ T2*) to obtain optimal sensitivity for BOLD changes. This leads to a net delay between excitation and acquisition. Significant gains can however be achieved in reverse spiral or related sequences,[31] or single-shot acquisitions at very high spatial resolution.[27] Note that, at higher field strength, this utilization can become more important as the necessary echo time to get T2*-weighted images reduces significantly. Also, T2*-related blurring for a given readout duration will increase at higher field strength. For this reason, several groups have performed preliminary work on the use of PI to get high spatial resolution single-shot EPI-based fMRI working at 3.0 T.[38,39] However, to fully profit from the increase in speed delivered by the reduction of echo-train length, one has to contemplate another class of sequences, which make more efficient use of the available time.

One such sequence that fulfills these criteria is the PRinciples of Echo-Shifting with a Train of Observations (PRESTO) sequence.[40] This three-dimensional sequence combines the echo-shifting technique[40] with multishot EPI readouts. Because of the reduced readout duration, its sensitivity to field inhomogeneities is reduced, as compared with conventional single-shot EPI readouts. Its main benefits are directly related to three-dimensional acquisition, which minimizes inflow artifacts[41] as well as spin history problems.[42] Furthermore, being a multishot EPI technique, PRESTO is less prone to image distortions.[22] On the other hand, the use of strong dephasing gradients combined with a multishot acquisition increases its motion sensitivity with respect to single-shot techniques.[43,44] Despite its advantages, PRESTO was never widely applied, mainly because of its limited temporal resolution. Nonetheless, the benefits of this sequence render it an ideal candidate for use with PI.[1] It has been shown that two distinct problems of PRESTO can be solved by combining it with SENSE. First, reducing the number of readouts has made PRESTO-SENSE the fastest BOLD fMRI sequence of its time, with whole-brain fMRI being performed in 1 second.[1] Then, reducing the number of shots of this sequence to only one per $k_x k_y$-plane rendered it less sensitive to motion artifacts and effectively reduced the temporal fluctuations with respect to the original PRESTO method. Figure 2 shows three reformatted planes of the original acquisitions on one volunteer with and without SENSE. Note the slight increase in apparent noise in the SENSE acquisition with respect to PRESTO.

Since the first paper, many people have worked on further improvement of this sequence. By simple optimization of the acquisition parameters, Arfanakis et al.[45] managed to use a very similar sequence at 1.5 T in a simple motor paradigm with a temporal resolution of 896 milliseconds.

Furthermore, by combining it with partial Fourier encoding,[46] Klarhofer et al. achieved an unprecedented temporal resolution of 500 milliseconds for a whole brain volume acquisition, with a temporal signal stability comparable to that of a full-Fourier, full-FOV EPI sequence. This sequence recently proved to be useful in detecting temporal differences among several activation sites in a visual-motor task.[47]

The drive for fast imaging techniques in fMRI comes probably from the fact that its sensitivity will depend on the temporal noise characteristics of the signal, including both slow and fast components. Very fast techniques provide the added benefit of being able to sample this high frequency noise, which can then be filtered out since it would be free from aliasing effects.[46] On the other hand, rapid imaging techniques

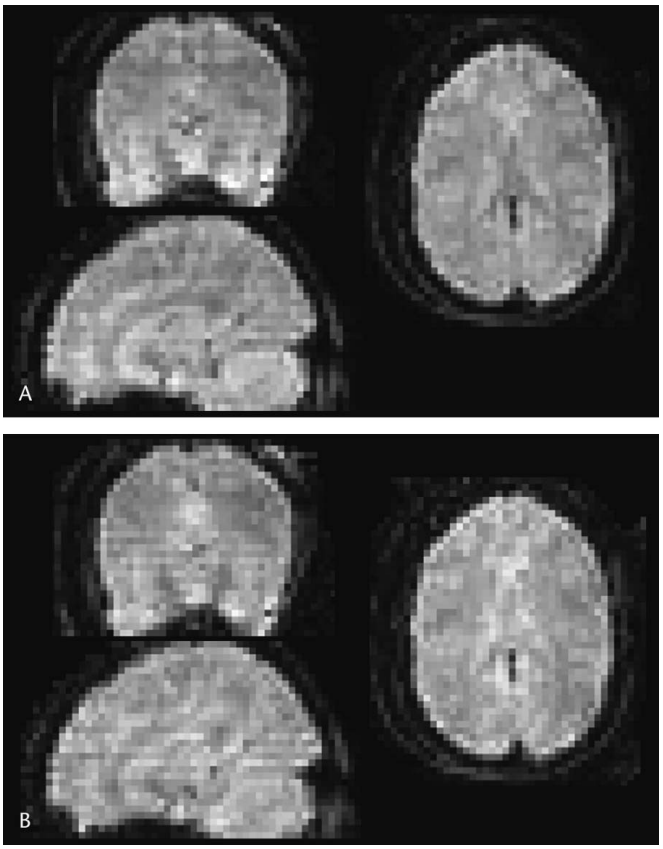

FIGURE 2. A, Conventional 3D-PRESTO images obtained at a temporal resolution of 2 seconds per volume (TR = 24 milliseconds, TE = 40 milliseconds, FA = 9°, 38 excited/30 reconstructed slices, FOV = 240 mm, rFOV = 80%, acquisition matrix = 64 × 48 × 38, two-shot EPI). B, PRESTO-SENSE images with identical parameters, except that a single-shot EPI readout/ $k_x k_y$ plane was used, resulting in a temporal resolution of 1s per volume. Both images are not averaged.

suffer from temporal correlations, as well as an inherently lower SNR. In a recent study, van der Schaaf et al.[46] used a Monte-Carlo analysis to demonstrate that the resulting interplay of these two effects turns out in favor of rapid techniques. This is in all likelihood related to the temporal stability of any fMRI series, which is mainly determined by the physiologic noise[48] (see also *SNR Considerations and Statistical Analysis*).

Finally, increased imaging speed can be essential when non-PI imaging strategies result in a temporal resolution too slow for a given application. One of the main problems in T2*-weighted BOLD fMRI is related to signal loss due to intravoxel dephasing near the air–tissue interfaces.[49] This effect comes from the presence of unwanted local field gradients, caused by magnetic susceptibility differences between tissue and air. Such effects are predominantly found near the sinuses and at the base of the brain. Several methods have been proposed in which an additional gradient encoding in the slice-selection direction is used to refocus the dephased magnetization,[50,51] thus reducing the signal loss. Among those methods, the GESEPI (Gradient-Echo Slice Excitation Profile Imaging) technique has been shown to be capable of removing distortions in the T2* relaxation characteristics, thereby correcting image-blurring and signal-loss-related artifacts. While GESEPI provides good reduction of these two kinds of artifacts, the utility of this technique for fMRI is limited due to its lengthy image acquisition time, as the through-plane gradient needs to be updated stepwise while the same imaging sequence is repeated. Recently, Yang et al.[52] proposed the use of SENSE to achieve a reasonable acquisition time (3.6 seconds for the acquisition of a 7-cm-thick slab), while Heberlein and Hu[53] demonstrated a similar utilization of PI using GRAPPA in a single-shot z-shimming technique. In both cases, PI combines particularly well with z-shimming methods, as it additionally reduces the blurring by reducing the readout length of the single-shot EPI readout.

Acoustic Noise Reduction with PI-fMRI

Modern MRI techniques rely on fast gradient switching to encode the signal. Recent developments in MRI gradient hardware have led to increases in the maximum achievable gradient amplitude and slew rate. The switching of gradients results in changing Lorentz forces on the gradient coil, leading to high levels of gradient acoustic noise. Especially in EPI, which is the most commonly used fMRI pulse sequence, the readout gradient results in high levels of scanner acoustic noise.[54] High sound pressure levels (SPLs) not only lead to patient discomfort and potential hearing damage but might also affect functional imaging experiments, especially those involving auditory stimulation.[55,56]

Various ways have been described in which SPLs in (functional) MRI can be reduced. A recent review by Moelker and Pattynama[55] describes these developments and the effects of acoustic noise in fMRI in detail. In brief, four different approaches can be distinguished: 1) The design of the gradient coil itself can be altered,[57] or SPL reduction can be achieved through modification of the mechanical characteristics of the gradient form by application of padding or alternative mounting strategies (eg, in vacuum[58]) of the gradients in the magnet. 2) At the patient level, either earplugs/earphones or an active sound canceling system[59] can be used. 3) The fMRI stimulus paradigm can be designed to avoid or minimize scanner acoustic noise interference, for example, through sparse temporal sampling.[56] 4) Finally, MRI pulse sequences can be designed to be quieter, specifically by altering the gradient wave forms design for EPI[60,61] or spiral readouts.[62] One recent suggestion within the scope of this paper is to use PI to achieve SPL reduction for a given acquisition window and spatial resolution.[63] The application of PI-MRI for SPL reduction is based on a significant reduction of the slew rate of the readout gradients. In EPI, the readout gradient is the dominant source of

gradient acoustic noise.[61] If the target spatial resolution and acquisition window duration remain the same, the ramp times of the readout gradient and the sampling bandwidth will be reduced by a factor of R for a rate-R SENSE acceleration factor. The factor-R reduced sampling bandwidth leads to a reduction of a factor R in readout gradient amplitude, therefore reducing the gradient slew rate by a factor R^2. Since the reduction in the number of samples is compensated by the decreased acquisition bandwidth, the image SNR is not expected to drop significantly, except for focal noise increase due to the SENSE g factor, which can be smaller than 10% depending on the number of coils, their configuration and the acceleration factor R (see *Dedicated Hardware*, above). Another advantage is that it can be used with virtually any scan technique and fMRI stimulus paradigm. Averaged over 3 scanner platforms (a 1.5 T Siemens and a 1.5 T and 3.0 T GE scanner), a SPL reduction of, respectively, 11.3 dB(A) (R = 2 SENSE, 4-fold slew rate reduction) and 16.5 dB(A) (R = 3 SENSE, 9-fold slew rate reduction) was achieved.[63] The average R = 3 SENSE SPL level equaled that of the average SPL measured with the readout gradient turned off completely, suggesting that the SPL in this case was predominantly caused by the other imaging gradients, which were unaltered in these experiments. No significant difference in both average t-value and temporal stability was found between conventional and "quiet" R = 2 SENSE fMRI experiments performed on 6 normal volunteers (10 experiments in total). A finger-tapping paradigm was used in these experiments, voxel size was 3.4 × 3.4 × 4.0 mm, and the average SENSE g factor was 1.04.

SNR Considerations and Statistical Analysis

As described by Pruessman et al.,[20] the image SNR in a SENSE MRI experiment is reduced by a factor $g\sqrt{R}$ when compared with the corresponding conventional experiment. In an fMRI experiment, however, the sensitivity for cerebral activation is only partially determined by the image SNR.[48] Temporal stability, expressed here by the temporal standard deviation (σ_t) ultimately determines statistical significance of the fMRI activation. Both the image noise σ_i and the physiologic noise (which is described here by the standard deviation of physiologic fluctuations, σ_{ph}) contribute to σ_t. Here it will be assumed that σ_i and σ_{ph} are fully independent and we can therefore describe σ_t as

$$\sigma_t = \sqrt{\sigma_{ph}^2 + \sigma_i^2}. \quad (2)$$

Only σ_i is directly affected by the reduced sampling in a PI-fMRI experiment, while σ_{ph} remains the same. As previously described, σ_i increases by $g\sqrt{R}$ in a rate-R SENSE experiment and therefore

$$\sigma_{t,SENSE} = \sqrt{\sigma_{ph}^2 + \sigma_{i,SENSE}^2} = \sqrt{\sigma_{ph}^2 + (g \cdot \sqrt{R} \cdot \sigma_{i,conventional})^2}, \quad (3)$$

where $\sigma_{i,conventional}$ is the intrinsic standard deviation in a given experiment without SENSE, and $\sigma_{t,SENSE}$ and $\sigma_{i,SENSE}$ are the temporal and intrinsic standard deviations in the corresponding SENSE experiment. This indicates that the penalty for SENSE use in fMRI depends on the relative contribution of physiologic noise to the overall temporal standard deviation:

$$\frac{\sigma_{t,SENSE}}{\sigma_{t,conventional}} = \sqrt{1 + (g^2 \cdot R - 1) \cdot \left(\frac{\sigma_{i,conventional}}{\sigma_{t,conventional}}\right)^2} \quad (4)$$

Therefore, the penalty for SENSE use in fMRI might not be as severe as one would expect based on a decrease in image SNR. In an experiment in which temporal signal stability is completely dominated by image SNR (and thus by σ_i), the measured fMRI activation does indeed suffer the full $g\sqrt{R}$ penalty ($\sigma_{t,SENSE}/\sigma_{t,conventional} = g\sqrt{R}$, see Eq. 4). On the other hand, if physiologic noise is the dominant noise source, application of SENSE will not affect the sensitivity of the fMRI experiment at all ($\sigma_{t,SENSE}/\sigma_{t,conventional} = 1$). This is demonstrated by Figure 3, which shows the temporal standard deviation increase in a R = 2 SENSE experiment for all voxels in the superior part of the brain of a normal volunteer performing a simple motor task.[48] Data are plotted as a function of the relative contribution of σ_i to the temporal standard deviation σ_t. The solid curve in this figure is the theoretical dependence of $\sigma_{t,SENSE}/\sigma_{t,conventional}$ on $\sigma_{i,conventional}/\sigma_{t,conventional}$ according

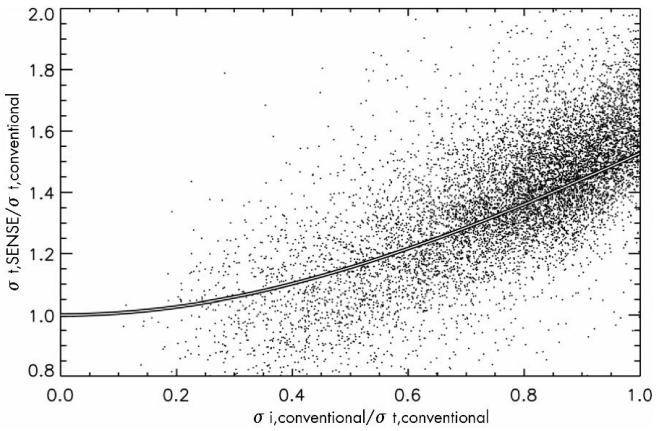

FIGURE 3. Plot of the temporal signal stability penalty incurred by the use of rate-2 SENSE for all pixels (·) in the superior brain of a volunteer. The solid line shows the predicted dependence of the relative contribution of intrinsic image noise to the overall temporal standard deviation as predicted by Eq. 4. In a voxel in which the intrinsic noise is the dominant noise source (*right side of the plot*), the penalty to the fMRI experiment is the factor $g\sqrt{2}$ predicted by Pruessmann et al.,[6] whereas fMRI sensitivity is completely unaffected by SENSE in voxels that are dominated by temporal instabilities (*left side of the plot*). Both a conventional single-shot gradient-echo EPI dataset and a similar rate-2 dataset were acquired with 3.4 × 3.4 × 4.0 mm voxels, using a 4-element dome coil.

to Eq. 4. This method can therefore be used to optimize spatial resolution for any given fMRI experiment.

OTHER FMRI TECHNIQUES

Vascular Space Occupancy (VASO)

In their study on the use of PI in spiral imaging, Weiger et al.[26] pointed out that PI acceleration factors have proven to be highly effective in reducing susceptibility artifacts at echo times much shorter than those used conventionally in BOLD fMRI. A technique was recently developed that allows noninvasive measurements of cerebral blood volume changes upon activation. This method, dubbed VASO,[64] is based on a simple nonselective inversion-recovery technique with an inversion time optimized to null the blood signal. Because of partial volume effects, the average signal in a voxel will then vary in amplitude depending on the amount of blood present in that voxel. Therefore, upon neuronal activation, the measured VASO signal will decrease due to the local vasodilation.[64] In such a method, one aims to use the shortest possible echo time, as any T2 or T2* weighting will reduce the potentially detectable VASO signal change due to the presence of residual BOLD effects,[65] which would result in a local signal increase. Therefore, partial Fourier acquisition is often used in conjunction with PI to get echo times well below 15 milliseconds.[65]

Furthermore, because of the use of nonselective inversion recovery pulses to null the blood signal, multislice imaging is not as simple as in BOLD fMRI. Recently, the same group came up with a method allowing Multiple Acquisitions with Global Inversion Cycling (MAGIC)[66] to render the VASO technique multislice capable. In short, this method is based on the repetitive use of nonselective inversion pulses to keep the blood signal nulled, while the tissue signal will decay from slice to slice with a time constant approximately equal to T1.[66] It is therefore imperative in this case to spend as little time as possible per single-slice acquisition to limit the slice-varying signal differences. In the first demonstration of its usefulness, MAGIC-VASO-SENSE was recently performed at 3T for retinotopic mapping in several volunteers.[67]

Arterial Spin Labeling (ASL)

Apart from BOLD, the other traditional technique used to detect activation is ASL (for a review, see Golay et al.[68]). For reasons similar to those discussed above for VASO, one would like to use the shortest possible echo time in ASL to avoid any contamination with residual BOLD signal.[69] Although this is not as crucial as in the VASO case, because of the possibility to acquire BOLD and perfusion-weighted images in an interleaved manner,[70] since the BOLD contributions can be eliminated by subtraction. Furthermore, in some of the most popular techniques available, such as the single-coil continuous ASL technique,[71,72] the use of a body coil as a transmit coil is seriously limited because of the necessary use of a long RF-labeling pulse for the flow-driven adiabatic labeling of the arterial magnetization. Therefore, the use of PI in ASL has been limited so far. However, there is great potential for these techniques at higher field strength,[73–75] since ASL will suffer then from the same problems related to magnetic field inhomogeneities as BOLD-based techniques.

The potential use of PI in ASL was recently demonstrated with an experiment in which FAIR (Flow-sensitive Alternating Inversion Recovery) was combined with VASO to measure the cerebral blood flow and cerebral blood volume changes in a graded visual activation experiment.[76] A typical activation map is shown in Figure 4 and overlaid onto the native VASO image in this case.

APPLICATIONS OF PI-BASED FMRI

Applications in Neuroscience

Apart from the studies mentioned earlier in this review (all of them using mostly simple primary motor or sensory activation), few studies have been published using PI-fMRI in cognitive neuroscience. There are several reasons for this. First, dedicated PI-optimized head coils have only recently

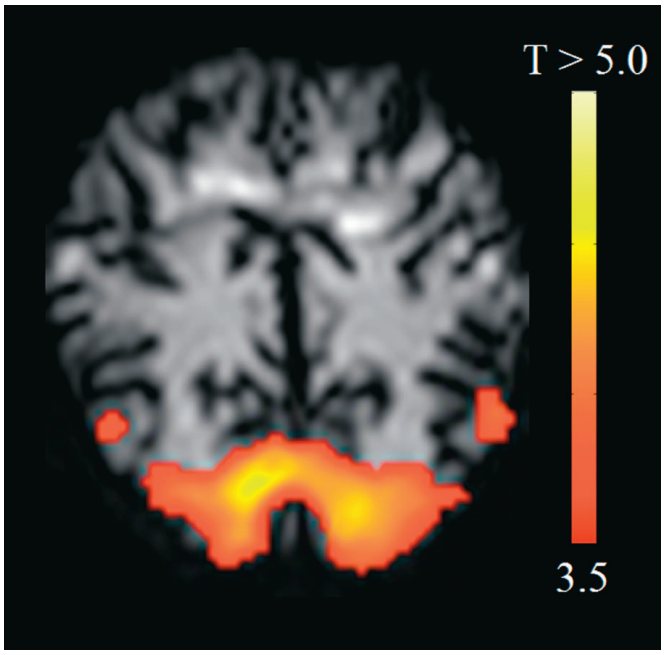

FIGURE 4. Example of a VASO-FAIR activation map, in which the detected signal changes are overlaid on a native SENSE-VASO image. The other parameters are: TR = 4 seconds, TI = 1 second (based on T_{1b} = 1680 ms at Hct = 0.38[90]), TE = 5.6 milliseconds, FA = 90°, FOV = 240 mm, slice thickness = 5 mm, matrix = 80 (reconstructed = 128), SENSE acceleration factor = 2, 60% reduced Fourier encoding, adiabatic (hyper-secant) inversion pulse.

made their entry into the portfolio of commercial MRI companies. Then, as demonstrated earlier, the direct benefits from the use of PI in fMRI are not so evident when working at 1.5 T using single-shot T2*-weighted EPI at the spatial resolution commonly used for fMRI. Generally, distortions are relatively small at this intermediate magnetic field strength and most vendors have EPI sequences that work well, needing very few, if any, corrections for distortions. However, with the recent arrival of clinical 3.0 T magnets in the field, there is an augmented concern about the increased spatial discrepancies between functional activation maps and the corresponding high-resolution T1-weighted images used as anatomic reference. Postprocessing techniques capable of reducing these distortions have been developed, often based on the concurrent acquisition of a B_0 field map.[77] However, in practice only few publications mention the use of such algorithms as a means to correct for distortions and blurring due to magnetic field inhomogeneities. PI allows neuroscience researchers to tackle the root of the problem by reducing distortions during data acquisition, therefore eliminating the need for heavy duty postprocessing algorithms.

In typical neuroscience applications of PI-fMRI, several groups working on the 3.0 T system at the Kennedy Krieger Institute (Baltimore, MD) have recently published cognitive neuroscience studies using SENSE-EPI data that were acquired with the following typical parameters[78–80]: TE = 30 milliseconds, FA = 90°, in plane resolution = 3 × 3 mm, 20 to 30 axial 3-mm-thick slices (depending on the required coverage), TR = 1.4-3.0 seconds. These studies were focused on the role of the medial temporal lobe in the encoding and retrieval of associative versus nonassociative memory,[78] on the control of object-based attention[79] or on the differences in activation between voluntary and stimulus-driven attentional control[80] in healthy volunteers.

Apart from these studies, other recent work has been published using similar paradigms, although sometimes using higher in-plane resolution. For example, Schmidt et al.[33] also used a learning paradigm to encode activation in the medial temporal lobe using 2.7 × 2.7 × 4 mm^3 resolution. Jansma et al.[81] used an even higher spatial resolution (1.75 × 1.75 × 3.5 mm^3) applied to a study of attention in the visual cortex. Finally, using more conventional imaging parameters, Wang et al.[82] studied the role of the hippocampus in the encoding and retrieval of short-term memory, Smits et al.[83] used SENSE-EPI at 3.0 T to study natural taste perception, while Peeters et al.[84] used GRAPPA-EPI to map activation in the anterior temporal lobe during semantic processing.

The common, interesting feature of almost all these studies is that their regions of interests are located near the base of the brain, where most distortions occur. Therefore, it is not altogether surprising to see such studies being among the first few to use PI-fMRI as a means to reduce distortion.

Clinical Applications

The authors were unable to find a single published study using PI-fMRI in the clinical environment. The reasons for this are probably similar to those stated for cognitive neuroscience studies, particularly the lack of an installed base of 3.0 T systems in clinical neuroradiological units that are factory equipped with both the hard- and software required to perform PI-fMRI studies. In the hospital of the National Neuroscience Institute in Singapore, PI-fMRI has been used in a number of cases over the course of the past year. In most cases, the paradigms used were simple visual, motor, or basic language tasks designed to locate the areas of activation in preparation for surgical procedures. The patient populations studied include, among others, patients with invasive tumors (mostly glioblastoma, grade III and higher) or patients with arteriovenous malformations. In these patients as well as those with epilepsy and hippocampal sclerosis, fMRI has been shown to be a useful tool for presurgical planning to preserve function and minimize patient morbidity.[85–87] fMRI has also been able to demonstrate reorganization and displacement of activated areas.[88,89] In these cases, PI was able to reduce the even stronger distortions due to magnetic susceptibility effects that are inherent in the imaging of the abnormal brain, such as hemorrhages and cavities. Imaging of inferior or basal structures like the sclerotic hippocampus in epilepsy also benefit from the reduction of signal dropout. In Figure 5, two representative cases imaged with PI-fMRI are shown, in which significantly activated areas are overlaid on either native EPI images or resliced onto high-resolution anatomic images.

CONCLUSION

The application of PI in fMRI is a relatively recent development and can still be considered to be in its infancy, as compared with the literature existing on the use of PI in cardiac imaging and other fields. However, recently available clinical 3.0 T scanners equipped with PI-capable hardware and software are bound to replace part of the current base of 1.5 T systems in most hospitals. This will lead to an increased application of PI-based fMRI techniques in applied research as well as in the clinical setting.

As summarized in this review, there are several benefits of PI for fMRI: from reduced artifacts related to magnetic field inhomogeneities in single-shot techniques to increased spatiotemporal coverage through reduced scanner acoustic noise. PI-fMRI appears to be an essential component to gather the maximal benefits of fMRI at high field strength. Since the performance of fMRI is limited by physiologic fluctuations as well as intrinsic image SNR, the sensitivity penalty for PI application in fMRI can be minimal. Depending on the application, PI-fMRI can play a role in the acquisition of fMRI data at the highest possible spatial or temporal resolution where physiologic fluctuations are still the dominant noise source.

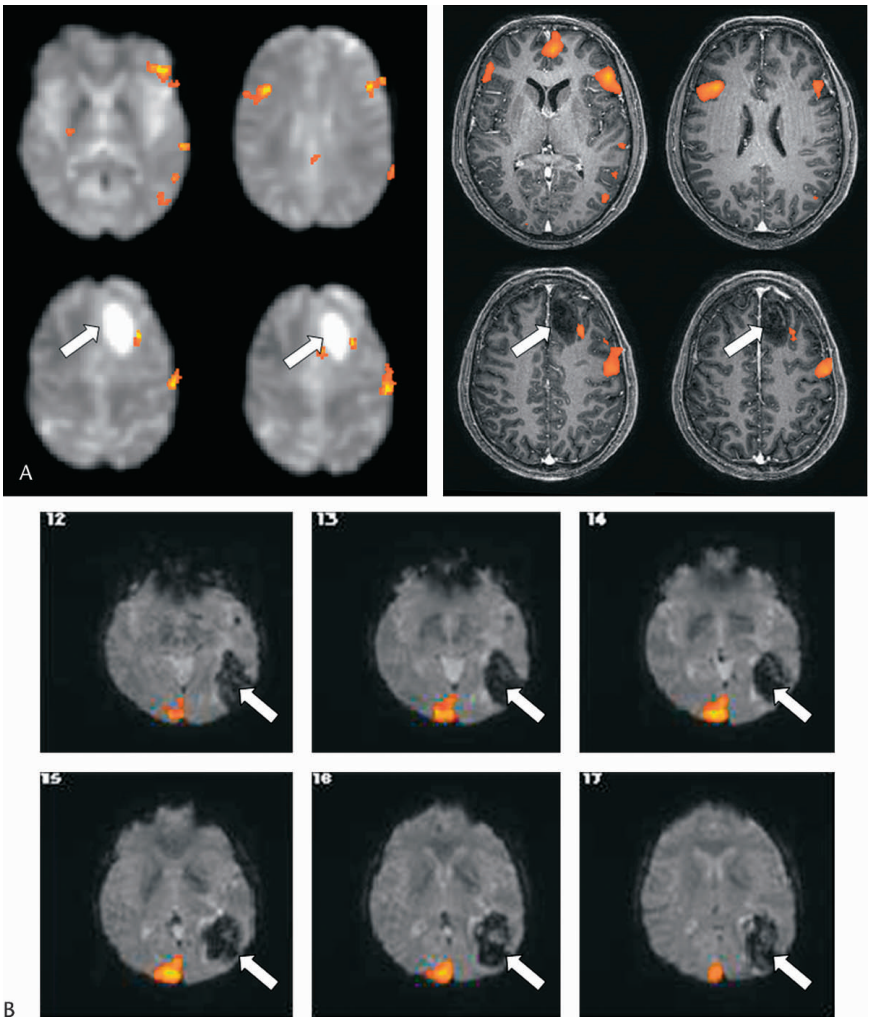

FIGURE 5. A, Presurgical fMRI language mapping in a patient with proven low-grade astrocytoma in the left superior frontal gyrus. (*Left*) fMRI activation map overlaid onto the SENSE-EPI images; (*Right*) fMRI activation map overlaid onto the post-contrast T1-weighted scan shows activation at the left Broca's and Wernicke's areas and the dorsolateral prefrontal cortex. Note the good correspondence between the activations overlaid on the native BOLD EPI images (*left*) and the high-resolution post-contrast T1-weighted anatomic scans (*right*). B, SENSE fMRI results from a 60-year-old woman with right homonymous hemianopia. The patient presented with an arteriovenous malformation at the inferior left parietal lobe, with recent hemorrhage and resultant large hematoma at the posterior left temporo-occipito-parietal lobe (*arrows*). During a simple visual task, activation was demonstrated only in the right occipital visual cortex with no activations in the left occipital cortex, correlating with her clinical findings. With parallel imaging, there was little image distortion despite the presence of blood products.

REFERENCES

1. Golay X, Pruessmann KP, Weiger M, et al. PRESTO-SENSE: an ultrafast whole-brain fMRI technique. *Magn Reson Med*. 2000;43:779–786.
2. Bammer R, Keeling SL, Augustin M, et al. Improved diffusion-weighted single-shot echo-planar imaging (EPI) in stroke using sensitivity encoding (SENSE). *Magn Reson Med*. 2001;46:548–554.
3. de Zwart JA, Ledden PJ, Kellman P, et al. Design of a SENSE-optimized high-sensitivity MRI receive coil for brain imaging. *Magn Reson Med*. 2002;47:1218–1227.
4. Roemer PB, Edelstein WA, Hayes CE, et al. The NMR phased array. *Magn Reson Med*. 1990;16:192–225.
5. de Zwart JA, Ledden PJ, van Gelderen P, et al. Signal-to-noise ratio and parallel imaging performance of a 16-channel receive-only brain coil array at 3.0 Tesla. *Magn Reson Med*. 2004;51:22–26.
6. Pruessmann KP, Weiger M, Scheidegger MB, et al. SENSE: sensitivity encoding for fast MRI. *Magn Reson Med*. 1999;42:952–962.
7. Yang Y, Spence DK, Petropoulos LS. Dedicated 12 element head array coil for parallel imaging applications at 3.0 Tesla. *Proceedings of the 10th ISMRM*. Hawaii, 2002:323.
8. Yang Y, Yang X, Petropoulos LS. A novel SENSE-optimized 8-channel hybrid transmit/phased array receive head coil for 3T and 4T horizontal systems. *Proceedings of the 11th ISMRM*. Toronto, 2003:468.
9. Wiggins GC, Triantafyllou C, Potthast A, et al. An 8 channel phased array coil and detunable TEM transmit coil for 7 T brain imaging. *Proceedings of the 12th ISMRM*. Kyoto, 2004:36.
10. Adriany G, Van de Moortele P, Wiesinger F, et al. Transceive stripline arrays for ultra high field parallel imaging applications. *Proceedings of the 11th ISMRM*. Toronto, 2003:474.
11. Moeller S, Van de Moortele P, Adriany G, et al. Parallel imaging performance for densely spaced coils in phase arrays at ultra high field strength. *Proceedings of the 12th ISMRM*. Kyoto, 2004:2388.
12. Zhang X, Liao Y, Zhu X-H, et al. An MTL coil array with a broad frequency tuning range for ultra-high field human MR applications from 3T to 7T. *Proceedings of the 12th ISMRM*. Kyoto, 2004:1602.
13. Junge S, Seifert F, Wuebbeler G, et al. Current sheet antenna array: a transmit/receive surface coil array for MRI at high fields. *Proceedings of the 12th ISMRM*. Kyoto, 2004:41.
14. Morris H, Seeber D. Multi-direction SENSE imaging using a head coil based on trianglular elements with a standard clinical scanner. *Proceedings of the 12th ISMRM*. Kyoto, 2004:1598.
15. Seeber D, Johnson W, Morris H. Eight-channel transmit/receive triangle coil for 3D SENSE. *Proceedings of the 12th ISMRM*. Kyoto, 2004:1593.
16. Iwadate Y, Boskamp EB, Nabetani A, et al. Design of an 8-channel head coil for SENSE acceleration in 2 directions. *Proceedings of the 12th ISMRM*. Kyoto, 2004:1613.
17. Weiger M, Pruessmann KP, Boesiger P. 2D SENSE for faster 3D MRI. *MAGMA*. 2002;14:10–19.
18. van der Schaaf A, Kahn R, Ramsey NF. Sensitivity benefits from ultra-fast fMRI: Monte Carlo analysis based on temporal noise in PRESTO-SENSE acquisitions. *Proceedings of the 12th ISMRM*. Kyoto, 2004:1031.

19. Sodickson DK, Manning WJ. Simultaneous acquisition of spatial harmonics (SMASH): fast imaging with radiofrequency coil arrays. *Magn Reson Med*. 1997;38:591–603.
20. Wiesinger F, Boesiger P, Pruessmann KP. Electrodynamics and ultimate SNR in parallel MR imaging. *Magn Reson Med*. In press.
21. Griswold MA, Jakob PM, Chen Q, et al. Resolution enhancement in single-shot imaging using simultaneous acquisition of spatial harmonics (SMASH). *Magn Reson Med*. 1999;41:1236–1245.
22. Farzaneh F, Riederer SJ, Pelc NJ. Analysis of T2 limitations and off-resonance effects on spatial resolution and artifacts in echo-planar imaging. *Magn Reson Med*. 1990;14:123–139.
23. Chen NK, Wyrwicz AM. Optimized distortion correction technique for echo planar imaging. *Magn Reson Med*. 2001;45:525–528.
24. Bammer R, Auer M, Keeling SL, et al. Diffusion tensor imaging using single-shot SENSE-EPI. *Magn Reson Med*. 2002;48:128–136.
25. Jaermann T, Crelier G, Pruessmann KP, et al. SENSE-DTI at 3 T. *Magn Reson Med*. 2004;51:230–236.
26. Weiger M, Pruessmann KP, Osterbauer R, et al. Sensitivity-encoded single-shot spiral imaging for reduced susceptibility artifacts in BOLD fMRI. *Magn Reson Med*. 2002;48:860–866.
27. Preibisch C, Pilatus U, Bunke J, et al. Functional MRI using sensitivity-encoded echo planar imaging (SENSE-EPI). *Neuroimage*. 2003;19:412–421.
28. Pruessmann KP, Weiger M, Bornert P, et al. Advances in sensitivity encoding with arbitrary k-space trajectories. *Magn Reson Med*. 2001;46:638–651.
29. Deichmann R, Gottfried JA, Hutton C, et al. Optimized EPI for fMRI studies of the orbitofrontal cortex. *Neuroimage*. 2003;19:430–441.
30. Tang H, Tabert MH, Albers M, et al. An optimized EPI pulse sequence using SENSE for fMRI studies of orbitofrontal and medial temporal brain areas. *Proceedings of the 12th ISMRM*. Kyoto, 2004:1029.
31. Stenger VA, Sutton BP, Boada FE, et al. Reversed spiral SENSE for fMRI. *Proceedings of the 12th ISMRM*. Kyoto, 2004:1024.
32. Ohliger MA, Grant AK, Sodickson DK. Ultimate intrinsic signal-to-noise ratio for parallel MRI: electromagnetic field considerations. *Magn Reson Med*. 2003;50:1018–1030.
33. Schmidt CF, Degonda N, Henke K, et al. Application of SENSE to fMRI studies of higher cognitive functions. *Proceedings of the 11th ISMRM*. Toronto, 2003:737.
34. Morgan PS, Kozel FA, George MS, et al. Optimal SENSE factor for BOLD fMRI at 3T. *Proceedings of the 12th ISMRM*. Kyoto, 2004:1030.
35. Little MW, Papadaki A, McRobbie DW. An investigation of GRAPPA in conjunction with fMRI of the occipital cortex at 3T. *Proceedings of the 12th ISMRM*. Kyoto, 2004:1025.
36. Griswold MA, Jakob PM, Heidemann RM, et al. Generalized autocalibrating partially parallel acquisitions (GRAPPA). *Magn Reson Med*. 2002;47:1202–1210.
37. Van de Moortele P, Adriany G, Moeller S, et al. Whole Brain fMRI in human at ultra-high field with parallel SENSE imaging. *Proceedings of the 12th ISMRM*. Kyoto, 2004:1027.
38. Schmidt CF, Pruessmann KP, Jaermann T, et al. High-resolution fMRI using SENSE at 3 Tesla. *Proceedings of the 10th ISMRM*. Hawaii, 2002:125.
39. Hoogenraad F, Rijckaert Y, Harvey PR, et al. High resolution ER-fMRI using SENSE at 3.0 Tesla. *Proceedings of the 10th ISMRM*. Hawaii, 2002:126.
40. Liu G, Sobering G, Duyn J, et al. A functional MRI technique combining principles of echo-shifting with a train of observations (PRESTO). *Magn Reson Med*. 1993;30:764–768.
41. Lu H, Golay X, van Zijl PC. Intervoxel heterogeneity of event-related functional magnetic resonance imaging responses as a function of T(1) weighting. *Neuroimage*. 2002;17:943–955.
42. Friston KJ, Williams S, Howard R, et al. Movement-related effects in fMRI time-series. *Magn Reson Med*. 1996;35:346–355.
43. Ramsey NF, van den Brink JS, van Muiswinkel AM, et al. Phase navigator correction in 3D fMRI improves detection of brain activation: quantitative assessment with a graded motor activation procedure. *Neuroimage*. 1998;8:240–248.
44. Jiang H, Golay X, van Zijl PC, et al. Origin and minimization of residual motion-related artifacts in navigator-corrected segmented diffusion-weighted EPI of the human brain. *Magn Reson Med*. 2002;47:818–822.
45. Arfanakis K, Heaton IA, Rogers BP, et al. Event-related fMRI with sub-second whole brain acquisition using 3D PRESTO-SENSE. *Proceedings of the 11th ISMRM*. Toronto, 2003:1750.
46. Klarhoefer M, Dilharreguy B, van Gelderen P, et al. A PRESTO-SENSE sequence with alternating partial-Fourier encoding for rapid susceptibility-weighted 3D MRI time series. *Magn Reson Med*. 2003;50:830–838.
47. Klarhoefer M, Dilharreguy B, Moonen CT. A rapid 3D partial-Fourier PRESTO-SENSE method for functional motor MRI. *Proceedings of the 12th ISMRM*. Kyoto, 2004:1070.
48. de Zwart JA, van Gelderen P, Kellman P, et al. Application of sensitivity-encoded echo-planar imaging for blood oxygen level-dependent functional brain imaging. *Magn Reson Med*. 2002;48:1011–1020.
49. Yablonskiy DA, Haacke EM. Theory of NMR signal behavior in magnetically inhomogeneous tissues: the static dephasing regime. *Magn Reson Med*. 1994;32:749–763.
50. Glover GH. 3D z-shim method for reduction of susceptibility effects in BOLD fMRI. *Magn Reson Med*. 1999;42:290–299.
51. Yang QX, Williams GD, Demeure RJ, et al. Removal of local field gradient artifacts in T2*-weighted images at high fields by gradient-echo slice excitation profile imaging. *Magn Reson Med*. 1998;39:402–409.
52. Yang QX, Smith MB, Wang J, et al. Reduction of magnetic field inhomogeneity artifacts in EPI with SENSE-GESEPI. *Proceedings of the 12th ISMRM*. Kyoto, 2004:2250.
53. Heberlein KA, Hu X. Improvements in single shot Z-shim using parallel imaging. *Proceedings of the 12th ISMRM*. Kyoto, 2004:2169.
54. Foster JR, Hall DA, Summerfield AQ, et al. Sound-level measurements and calculations of safe noise dosage during EPI at 3 T. *J Magn Reson Imaging*. 2000;12:157–163.
55. Moelker A, Pattynama PM. Acoustic noise concerns in functional magnetic resonance imaging. *Hum Brain Mapp*. 2003;20:123–141.
56. Hall DA, Haggard MP, Akeroyd MA, et al. Sparse temporal sampling in auditory fMRI. *Hum Brain Mapp*. 1999;7:213–223.
57. Mansfield P, Chapman BL, Bowtell R, et al. Active acoustic screening: reduction of noise in gradient coils by Lorentz force balancing. *Magn Reson Med*. 1995;33:276–281.
58. Katsunuma A, Takamori H, Sakakura Y, et al. Quiet MRI with novel acoustic noise reduction. *MAGMA*. 2002;13:139–144.
59. Goldman AM, Gossman WE, Friedlander PC. Reduction of sound levels with antinoise in MR imaging. *Radiology*. 1989;173:549–550.
60. Loenneker T, Hennel F, Ludwig U, et al. Silent BOLD imaging. *MAGMA*. 2001;13:76–81.
61. Hennel F, Girard F, Loenneker T. Silent MRI with soft gradient pulses. *Magn Reson Med*. 1999;42:6–10.
62. Oesterle C, Hennel F, Hennig J. Quiet imaging with interleaved spiral read-out. *Magn Reson Imaging*. 2001;19:1333–1337.
63. de Zwart JA, van Gelderen P, Kellman P, et al. Reduction of gradient acoustic noise in MRI using SENSE-EPI. *Neuroimage*. 2002;16:1151–1155.
64. Lu H, Golay X, Pekar JJ, et al. Functional magnetic resonance imaging based on changes in vascular space occupancy. *Magn Reson Med*. 2003;50:263–274.
65. Lu H, van Zijl PC. Experimental separation of intra and extravascular BOLD effects using multi-echo VASO and BOLD fMRI at 1.5T and 3.0T. *Proceedings of the 12th ISMRM*. Kyoto, 2004:275.
66. Lu H, van Zijl PC, Hendrikse J, et al. Multiple acquisitions with global inversion cycling (MAGIC): a multislice technique for vascular-space-occupancy dependent fMRI. *Magn Reson Med*. 2004;51:9–15.
67. Lu H, Basso G, Serences JT, et al. Retinotopic mapping in human visual cortex using Vascular-Space-Occupancy (VASO) dependent fMRI. *Proceedings of the 12th ISMRM*. Kyoto, 2004:115.
68. Golay X, Hendrikse J, Lim TC. Perfusion imaging using arterial spin labeling. *Top Magn Reson Imaging*. 2004;15:10–27.
69. Kim SG, Tsekos NV, Ashe J. Multi-slice perfusion-based functional MRI using the FAIR technique: comparison of CBF and BOLD effects. *NMR Biomed*. 1997;10:191–196.

70. Wong EC, Buxton RB, Frank LR. Implementation of quantitative perfusion imaging techniques for functional brain mapping using pulsed arterial spin labeling. *NMR Biomed*. 1997;10:237–249.
71. Alsop DC, Detre JA. Multisection cerebral blood flow MR imaging with continuous arterial spin labeling. *Radiology*. 1998;208:410–416.
72. Gonzalez-At JB, Alsop DC, Detre JA. Cerebral perfusion and arterial transit time changes during task activation determined with continuous arterial spin labeling. *Magn Reson Med*. 2000;43:739–746.
73. Franke C, van Dorsten FA, Olah L, et al. Arterial spin tagging perfusion imaging of rat brain: dependency on magnetic field strength. *Magn Reson Imaging*. 2000;18:1109–1113.
74. Wang J, Alsop DC, Li L, et al. Comparison of quantitative perfusion imaging using arterial spin labeling at 1.5 and 4.0 Tesla. *Magn Reson Med*. 2002;48:242–254.
75. Yongbi MN, Fera F, Yang Y, et al. Pulsed arterial spin labeling: comparison of multisection baseline and functional MR imaging perfusion signal at 1.5 and 3.0 T: initial results in six subjects. *Radiology*. 2002;222:569–575.
76. Golay X, Lu H, Hong WT, et al. Simultaneous measurements of CBV and CBF changes using VASO-FAIR. *Proceedings of the 12th ISMRM*. Kyoto, 2004:720.
77. Jezzard P, Clare S. Sources of distortion in functional MRI data. *Hum Brain Mapp*. 1999;8:80–85.
78. Kirwan CB, Stark CE. Medial temporal lobe activation during encoding and retrieval of novel face-name pairs. *Hippocampus*. In press.
79. Serences JT, Schwarzbach J, Courtney SM, et al. Control of object based attention in human cortex. *Cereb Cortex*. In press.
80. Serences JT, Shomstein S, Leber AB, et al. Coordination of voluntary and stimulus-driven attentional control in human cortex. In press.
81. Jansma JM, van Gelderen P, de Zwart JA, et al. A stimulus design allowing separation of main and interaction effects applied to a visual attention task. *Proceedings of the 12th ISMRM*. Kyoto, 2004:402.
82. Wang J, Eslinger PJ, Meadowcroft M, et al. Different patterns of visual cortex and hippocampal activation during encoding and retrieval of face-name pairs. *Proceedings of the 12th ISMRM*. Kyoto, 2004:1153.
83. Smits M, Peeters RR, Van Hecke P, et al. A 3T event-related fMRI study of natural taste perception. *Proceedings of the 12th ISMRM*. Kyoto, 2004:1051.
84. Peeters RR, Vandenbulcke M, Vandenberghe R, et al. Visualizing anterior temporal activation during semantic processing with parallel imaging techniques. *Proceedings of the 12th ISMRM*. Kyoto, 2004:736.
85. Sitoh YY, Tien RD. Neuroimaging in epilepsy. *J Magn Reson Imaging*. 1998;8:277–288.
86. Lee CC, Ward HA, Sharbrough FW, et al. Assessment of functional MR imaging in neurosurgical planning. *AJNR Am J Neuroradiol*. 1999;20:1511–1519.
87. Thulborn KR, Davis D, Erb P, et al. Clinical fMRI: implementation and experience. *Neuroimage*. 1996;4(suppl):101–107.
88. Kollias SS, Landau K, Khan N, et al. Functional evaluation using magnetic resonance imaging of the visual cortex in patients with retrochiasmatic lesions. *J Neurosurg*. 1998;89:780–790.
89. Alkadhi H, Kollias SS, Crelier GR, et al. Plasticity of the human motor cortex in patients with arteriovenous malformations: a functional MR imaging study. *AJNR Am J Neuroradiol*. 2000;21:1423–1433.
90. Lu H, Clingman C, Golay X, et al. What is the longitudinal relaxation time (T1) of blood at 3.0 Tesla? *Proceedings of the 11th ISMRM*. Toronto, 2003:669.

